One step forward passive baseline-free imaging using nonlinear secondary noise sources

Lynda Chehami, Marina Terzi, Emmanuel Moulin, E. Chatelet, Francesco Massi, Julien de Rosny

One step forward passive baseline-free imaging using nonlinear secondary noise sources

Lynda Chehami[1], Marina Terzi[2], Emmanuel Moulin[1], Eric Chatelet[3], Francesco Massi[4], Julien de Rosny[5]

[1]Univ. Polytechnique Hauts de France, CNRS, Univ. Lille, UMR 8520-IEMN-Institut d'Electronique de Microélectronique et de Nanotechnologie, F-59313 Valenciennes, France
[2]Laboratoire d'Acoustique de l'Université du Mans, Av. Olivier Messiaen, 72085 Le Mans, France
[3]LaMCoS UMR CNRS 5259, INSA University of Lyon, F69621 Lyon Cedex, France
[4]University of Rome 'La Sapienza' – Department of Mechanical and Aerospace Engineering, 00184 Rome, Italy
[5]Institut Langevin UMR CNRS 7587, ESPCI ParisTech, F75231 Paris Cedex 05, France

E-mail: [1]lynda.chehami@uphf.fr

Abstract. This paper introduces the concept of secondary noise sources for passive defect localization in structures. The proposed solution allows for the exploitation of the principle of Green's function retrieval from noise correlation, even in the absence of an adequate ambient noise. The main principle is to convert a part of low-frequency modal vibrations into high-frequency noise by exploiting the frictional contact nonlinearities. The device consists of a mass-spring resonator coupled to a flexible beam by a rough frictional interface. The extremity of the beam, attached to the surface of a plate, excites efficiently flexural waves in the plate up to 30 kHz when the primary resonator vibrates around its natural frequency, i.e. a few dozens Hz. A set of such devices is placed at random positions on the plate surface, and low-frequency excitation is provided by a shaker. The generated high-frequency noise is recorded by an array of eight piezoelectric transducers attached to the plate. A differential correlation matrix is constructed by subtracting correlation functions computed from noise signals at each sensor pairs, before and after the introduction of a local heterogeneity mimicking a defect. Then dispersive beamforming is applied on the differential correlation matrix to locate the defect. This technique shows good results for linear defects, but refers to a measurement on a baseline healthy sample, which can be strongly affected by environmental conditions. In this context, we propose, in second part, an acoustic reference-free method for localizing defects in thin plates. The new approach is based on the combination of pump-probe measurements and beamforming imaging. The pump-probe scheme here means the simultaneous excitation of low-frequency vibrations and high-frequency acoustic pulses generated by a piezoelectric transducer and recorded by an array of sensors. The role of pumping vibrations is in imposing changes to loading conditions for a defect (here a model Hertzian contact i.e. a small ball pressed against the tested plate) while the ultrasonic Lamb wave pulses probe the defect in various loading states. Then beamforming algorithm is used to detect and locate the origin of modulation.

1. Introduction

Theoretical and experimental studies have shown that, under the assumption of diffuse noise, the cross-correlation of the recorded fields in two points A and B of a medium gives access to the impulse response between these points as if one receiver acted as an active

source [1, 2, 3, 4, 5, 6, 7]. The mathematical expression associated to this property can be written as

$$C_{ij} = D_{ij} + n_{ij}\,, \tag{1}$$

where D_{ij} represents a deterministic term containing causal and anticausal parts of the Green's function between two receiver locations R_i and R_j and n_{ij} is a residual noise term or Green's function reconstruction error.

In ultrasound applications, particularly in structural health monitoring (SHM) field, power consumption and complexity of the electronics might represent key issues for the standard methods used in active configurations (pitch-catch). An alternative way could then consist in analyzing the Green's functions estimated passively, using the physical principle illustrated by Eq. (1), in order to reveal defects (cracks, holes...). Here passive means that no artificially-driven acoustic (ultrasound) sources are used.

The possibility of detecting and localizing defects using ambient noise (friction noise, acoustic noise...) more or less uniformly generated on surface plates has been demonstrated numerically and experimentally in recent works [8, 9]. Suitable noise sources for this application have to be uncorrelated, spatially stationary and with frequency contents in the ultrasound range. Such source characteristics might not be often available in a natural way. On the other hand, low frequency vibrations sources are common in a lot of situations (transportation...). These sources preferentially excite the first structural modes. Since they are very low frequency, strongly correlated from a point to another and possibly non-stationary, such vibrations cannot be used for the passive defect localization application. In comparison to more traditional active methods, the main expected advantage is lower resource requirements in terms of power consumption, hardware, etc. To overcome this problem, we propose here a prototype of an artificial secondary "passive" acoustic source. Its role is to transfer part of the energy from the ambient low frequency (LF) vibrations to a secondary high frequency (HF) field by exploiting the frictional contact nonlinearities. In other hand, the applicability of uncontrolled noise used for defect detection based on linear responses is not sufficiently sensitive to crack-type defects (cracks, delaminations, debonding) which are most crucial in terms of structure performance. In addition, linear SHM methods require baseline subtraction that eventually results in the lack of long-term robustness (e.g. strong temperature-induced biases). In recent years, nonlinear ultrasound methods have proven to be very sensitive to structural damage [10] even at its onset. Therefore, the objective here is to develop nonlinear (NL) passive techniques for damage detection that would represent a new step in SHM.

This paper is organized as follows: In section 2, the concept and the preliminary characterization of the proposed artificial secondary sources devices are presented. Then, in section 3, we propose a baseline free passive imaging technique for contact defects detection. Finally, some conclusions are presented in section 4.

2. Nonlinear secondary noise sources

In order to extend the application range of the correlation technique used in passive imaging, we shown previously [11, 12] that the development of multi-resonators systems with frictional surfaces allowed for producing a secondary acoustic field used for passive SHM techniques. Figures 1-(left) and 1-(right) show a photography of the artificial device and its simulated model, respectively.

The designed device consists in a mechanical system composed by two resonators connected by a frictional interface. The primary resonator is a mere spring-mass oscillator, whose natural

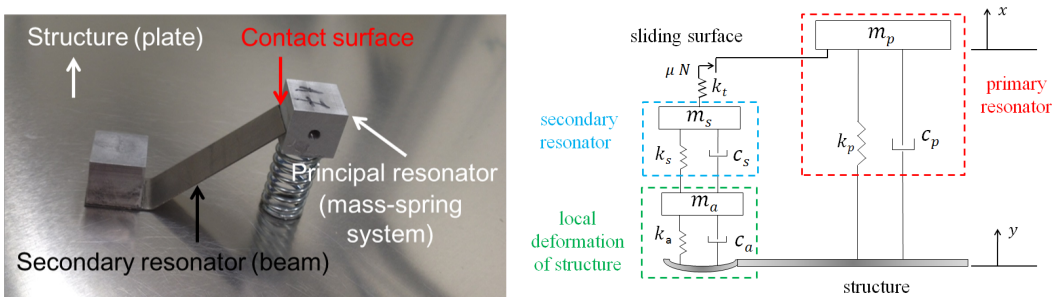

Figure 1. (left) Photography of the proposed device with principal resonator corresponding to a spring-mass system. (right) simplified 3 degrees-of-freedom model for simulating the energy transfer by frictional contact.

frequency is tuned to the low frequency (LF) structural vibrations of the structure (plate). The lateral surface of the mass, oscillating along the vertical direction, interacts by dry frictional contact with the tip of the beam, which is the secondary resonator. This secondary resonator is a flexible beam with one side in frictional contact with the mass of the first resonator and its opposite side rigidly bonded on the structure. The vibration of the primary resonator, induced by the ambient LF field, allows frictional sliding at the contact surface with the secondary resonator. In such a way a part of the LF vibratory energy is transferred to the secondary resonator by the random excitation at the frictional contact interface. This nonlinear interaction will then excite the modes of the clamped beam over a wide frequency range, depending on the contact characteristics such as roughness, static contact force, relative velocity of the sliding solids, and so on. Finaly, part of the vibratory energy of the second resonator will leak into the plate in the form of plate waves, thus constituting a secondary acoustic field in the plate. The characteristics of contact-induced vibrations in the presence of roughness [13, 11] allow to expect the presence of frequency components compatible with the application in the secondary field (typically a few kHz to a few dozens kHz). The working principle of this device can be explained and modeled [11] by considering the three degrees-of-freedom system presented in Figure. 1-(right). m_p, m_s and m_a are lumped masses accounting for the masses of the primary and secondary resonators and of the locally deformed structure. k_p, k_s and k_a are the corresponding lumped stiffness. C_p, C_s and C_a are the viscous damping coefficients for the primary and secondary resonators and the local deformation of the structure, respectively. Finally, the dry contact friction is modeled by a slider element with tangential constant stiffness k_t (macroslip model associated to a node to node contact element). Thanks to the nonlinearities of friction, generated mainly during the "slipping", and introduced into the model by the nonlinear contact force, the primary resonator is coupled to the second resonator, which responds with its own resonance, transferring energy to the structure at its frequency. In this work, the acoustic signals generated by the secondary sources are measured experimentally using a set of piezoelectric transducers.

2.1. Experimental characterization of artificial sources and their use in passive imaging

The experimental setup consists on a thin plate of 1 m × 1 m and 3-mm thick, made of aluminum (see Figure. 2-(left)). Low frequency excitation is provided by a shaker attached at a point of the plate surface. Twelve nonlinear secondary acoustic source devices (S_1, ..., S_{12}) have been glued on the plate, at arbitrary positions. An experimental characterization of the frequency content of the secondary field generated by the devices is performed. In a first experiment, the relative motion between the primary and secondary resonators at the contact interface has been avoided on all the devices by adding a sheet of paper between the mass surface and the contacting tip of the beam. This action will be referred to as "deactivating" the nonlinear

secondary source devices, because it avoids the sliding and thus the wideband excitation coming from the frictional contact. Then, the shaker is excited with a white noise in the frequency band [70, 150] Hz. The average power spectral density of the signals recorded on the transducers is plotted on Figure. 2-(right) (black curve) in logarithmic scale, as a function of frequency.

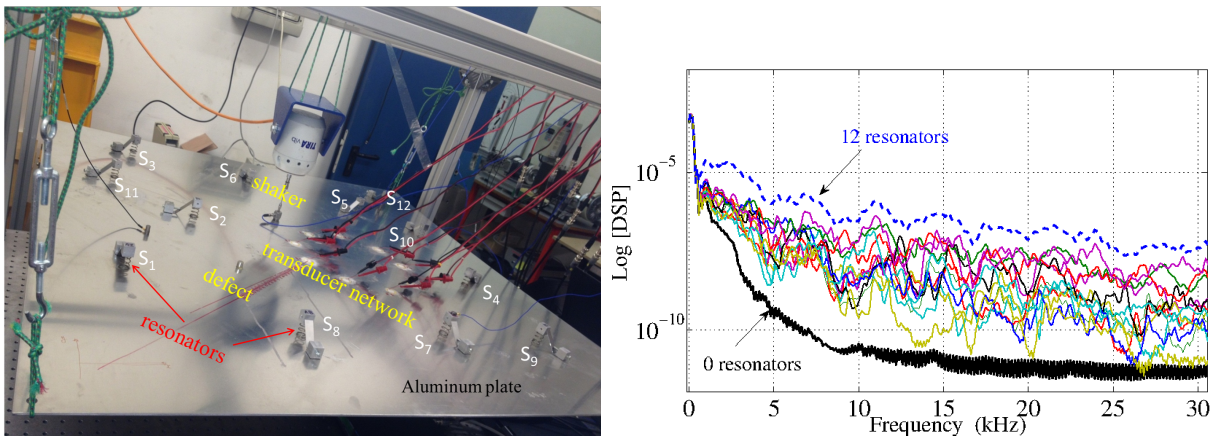

Figure 2. Experimental setup: (left) Photography of the experimental setup, (right) Averaged power spectral density (PSD) of recorded noise with: all resonators deactivated (black line), all resonators activated (blue dashed curve) and each resonator activated separately (other curves).

As expected, only the low frequency components excited by the shaker are significant. The same measurement is performed when reactivating the twelve resonators (blue dashed curve), i. e. when allowing the sliding at the contact by removing the paper. Significant acoustic power appears now in the frequency band [5, 30] kHz, approximately five orders of magnitude higher than the noise level shown by the black curve. These results essentially validate the LF to HF conversion principle. However, similar measurements performed with each single resonator activated at a time (thin colored curves) show a great dispersion in their HF generation behaviors. The convenience of the HF secondary noise for the defect localization technique based on passive noise correlation is then verified. To do so, acoustic signals are recorded on the receivers array (R1, . . . , R8) for both cases with and without defect. The raw signals are first frequency whitened between 0.5 kHz and 30 kHz [**?**]. Then the differential correlation matrix $\mathbf{\Delta C}$ is computed and used for imaging. For experimental repeatability purpose, the considered defect is a pair of cylindrical magnets (diameter 9 mm, height 10 mm) facing each other on the opposite sides of the plate and coupled to the plate with honey.

The principle of the imaging algorithm used here consists in back-propagating each element of indexes (i, j) of the matrix $\mathbf{\Delta C}$ according to the current pixel position (x, y). The back-propagation function (bpf) of $\mathbf{\Delta C}$ is given by [8]

$$\mathrm{bpf}_{(x,y)}(\omega) = \sum_{i=1,j=1(i\neq j)}^{N_R,N_R} \mathbf{\Delta C}_{ij}(\omega)\, e^{j\,[d_i(x,y)+d_j(x,y)]\,k(\omega)}, \tag{2}$$

where $d_i(x, y)$ is the distance between the i^{th} receiver and the pixel at position (x, y), $k(\omega)$ is the wave number of the Lamb mode A_0, $\mathbf{\Delta C}_{ij}(\omega)$ is the Fourier transform of $\mathbf{\Delta C}_{ij}(t)$ and N_R is the number of elements in the array (eight in this example). The bpf function leads to a constructive sum and a maximum of the pixel intensity on the defect location [8]. As for pixels located elsewhere, the obtained intensity is made up of a summation of non-coherent contributions (including correlation residues, reverberated wavepackets, grating lobes).

The obtained results when all the secondary sources S_1 to S_{12} are reactivated, by allowing the frictional sliding at their contacting interfaces, are shown on Figure. 3 for two defect positions.

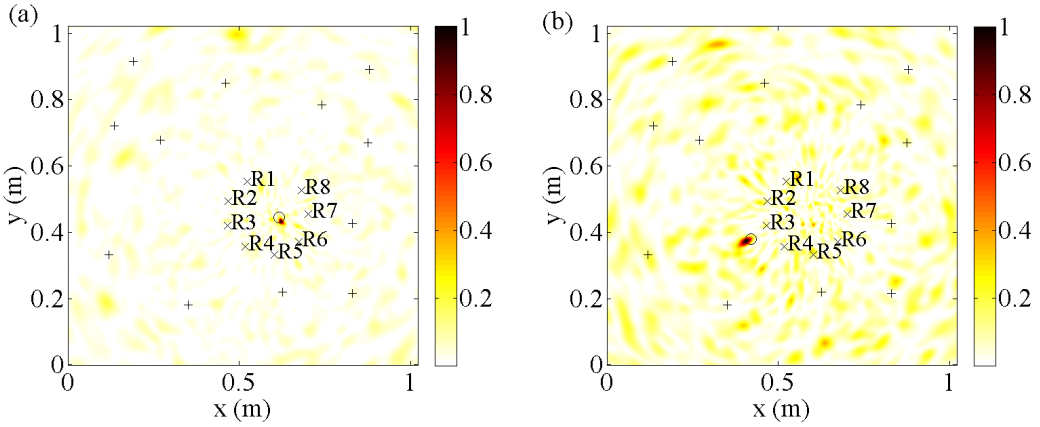

Figure 3. Defect localization images obtained with all secondary sources (S_1 to S_{12} indicated by '+') activated: (a) Defect outside receivers array, (b) Defect outside receivers array. The defect position indicated by a black circle.

The quality of Fig. 3-(a), where the defect is inside the network, is better than Fig. 3-(b), where the defect is outside. This effect, also observed with classical HF noise sources [9], is directly related to the effective aperture of the sensors array versus the defect position.

As shown here, the applicability of uncontrolled noise for linear defect detection applications in plates is very promising. However, detection based on linear responses is not sufficiently sensitive to crack-type defects (cracks, delaminations, debonding) which are most crucial in terms of structure performance. In addition, linear SHM methods require baseline subtraction that eventually results in the lack of long-term robustness (e. g. strong temperature-induced biases). Therefore, in next section we will present a new alternative method based on nonlinear (NL) passive techniques for damage detection that would represent a new step for SHM applications.

3. Baseline-free imaging using pump-probe techniques

This section describes preliminary passive pump-probe experiments. The pump-probe technique here consists to excite the material simultaneously by pump wave (LF) and probe wave (HF). The idea behind this is that LF vibrations will slightly modulate the contact condition (contact load, relative positions) between the plate and the defect. Each recorded HF signal, containing components with wave paths having crossed the contact area, will then carry information on the contact state at the instant of measurement.

3.1. Experiment with a set of controlled simultaneously emitting white noise sources

The same aluminum plate used previously in section 2 is used here for pump-probe experiments, with a contact acoustic nonlinearity in a form of 1 cm steel sphere pressed against the plate is excited by harmonic continuous pump wave. High frequency white noise plays the role of a probe signal. The mix of high frequency noise and pump wave is recorded by the set of PZT patches glued on the top surface of the plate. To retrieve Green's function from noise correlation, we need homogeneously distributed acoustic diffuse field with wide band of frequencies. For this purpose, we use a set of $N_s = 14$ PZT sources of the same kind as $N_r = 14$ receivers distributed on the top surface of the plate. They emit uncorrelated Gaussian white noise simultaneously of

40 s duration. Both emission and reception are operated with a multichannel digital sampling board (24 I/O MOTU, 96 kS/s, 24 bits digitizer). The shaker firmly attached to the plate emits a continuous sine wave at $f_{pump} = 1$ Hz (see Figure. 4).

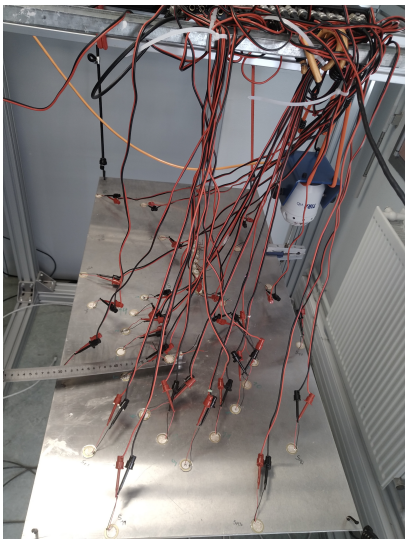

Figure 4. Passive experimental setup with multiple simultaneous noise sources.

Noise spectral range for emission is between 1 and 30 kHz where A0 Lamb mode is dominant. For every recording, low-pass filtering is applied to retrieve the LF pump vibration $s_{pump}(t)$. As for the high frequency signal, band-pass filtering between 1 and 30 kHz is applied, followed by a whitening procedure consisting in temporal and spectral normalization. To made the defect imaging, whitened signal received at the n^{th} sensor is cut into M short slices of duration $\Delta T \ll 1/f_{pump}$ smoothed with Hanning window. Each slice represents a particular contact loading state. Indeed, since ΔT is much smaller than the LF period, as pointed out above, the contact state can be assumed stationary during one HF signal slice. Since the effect of contact modulation in the HF signals is expected to be slight, we seek to cumulate information acquired at different contact states (i.e. different HF signal slices). The post-processing used here is similar to what described in [14] but adapted to passive case.
Let us denote $s_{n,m}(t)$ the m^{th} slice of a signal recorded by the receiver R_n. Instead of actual emitter in active experiments, one of the receivers R_{VE} plays the role of a virtual emitter. Then for the m^{th} slice and receiver R_n, cross-correlation $C_{n,m}$ between signal recorded by this receiver $s_{n,m}$ and signal recorded by virtual emitter $s_{VE,m}$ is computed. As a result for each slice, N_r correlations are obtained. Differential correlations for the m^{th} slice and n^{th} receiver are then defined as follows

$$\Delta C_{n,m}(t) = C_{n,m}(t) - \frac{1}{M}\sum_{m=1}^{M} C_{n,m}(t)\,. \tag{3}$$

Then back-propagation procedure used previously in section 1 is applied to this differential correlation. Coherent imaging results with synchronous detection (with pump amplitude weighting coefficients) are shown on Figure. 5.

The obtained result is not satisfactory as the defect is not localized. To understand the reasons of such a low image contrast, the current experimental parameters are briefly analyzed below and ways of improvement are proposed.

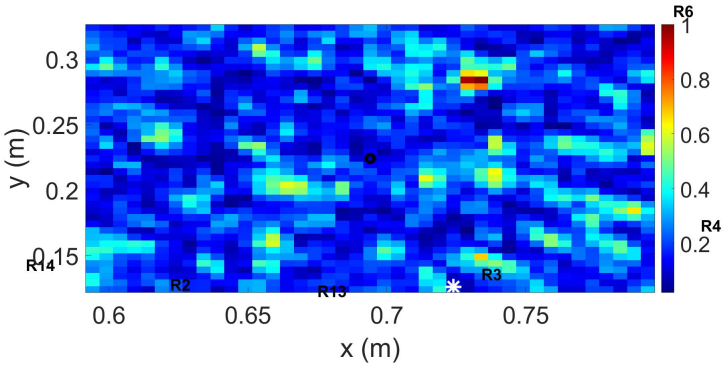

Figure 5. Localization result for passive pump-probe experiment $N_s = 14$ simultaneously emitting uncorrelated noise sources. $N_r = 14$.

3.2. Contrast improvement

It has been shown in previous works [15] that accuracy of the Green's function reconstruction can be evaluated by means of relative noise level RNL defined as

$$RNL = \frac{\int n_{ij}^2(t)dt}{\int D_{ij}^2(t)dt}, \tag{4}$$

which represents physically a ratio of energy between the reconstruction error and the deterministic part of the GF. Here RNL estimation might help us answer the question whether it is hypothetically possible to localize a defect with a given scattering cross-section under given experimental conditions (plate geometry and number of noise sources) using back-propagation algorithm. In this context, it is shown that for the reverberated signals in plates RNL can be expressed as follows [15]:

$$RNL = \frac{1}{N_s}(\frac{5}{4} + \frac{2\pi\eta_0}{\tau}), \tag{5}$$

where N_s is number of noise sources, τ is attenuation time related to exponential decay of reverberated signals, η_0 is the plate modal density.

Indeed, $n_{i,j}$ in Eq. (1) is not an actual noise, but a (deterministic) reconstruction error related to the number (and location) of the noise sources, as explained in [15]. The back-propagation of them associated to summation over receivers, will not result in independent terms for different defect states m, since noise sources are the same for all states. Therefore, here coherent summation over m will not reduce noise. To understand better, the detection contrast is evaluated theoretically one considering that $n(t)$ is a zero-mean additive Gaussian noise with variance σ_n^2 affecting the recorded ultrasonic signals. Presence of this noise will result in a non-zero, speckle-like, background on the images, even in the absence of a defect. It is shown in [16], that the corresponding contrast expression can be written as

$$C = \gamma\chi'\bar{\sigma}_0, \tag{6}$$

with γ is a term related to the geometrical configuration of the sensor network, χ' corresponding here to the signal-to-noise ratio associated to the passive Green's function reconstruction, which is quantified by the inverse of RNL, and $\bar{\sigma}_0$ is the scattering cross-section of the defect.

In the presence of a defect, the Green's function reconstruction error will not only depends on the plate properties, but also on the defect features. Formally, this reconstruction error when the defect is in a given state m can be written as

$$n_{ij,m} = n_{ij,0} + \delta n_{ij,m}\,, \tag{7}$$

where $n_{ij,0}$ is the Green's function reconstruction noise when the defect is in the state taken as reference (average over a pump period here).

Then we can define the RNL related to the modulation of the defect by the pump as

$$\delta RNL = \frac{\int \delta n_{ij,m}^2(t)dt}{\int D_{ij}^2(t)dt} \tag{8}$$

and then $\chi' = 1/\delta RNL$ in the contrast expression Eq. (6).

Estimation of δRNL requires further theoretical work in perspective. However, remarking that χ' is homogeneous to inverse of RNL, and that RNL is itself homogeneous to inverse of the number of sources N_s (from Eq. (5)), it seems reasonable to assume proportionality between χ' and N_s. To conclude, in the current passive reference-free experiment defect is not detected using Green's function reconstruction. Nevertheless, based on Eq. (6), we can increase the image contrast by:

- Increasing χ' (decreasing RNL and δRNL) by augmenting number of noise sources N_s.
- Increasing γ by augmenting number of receivers N_r.
- Increasing the defect scattering cross-section $\bar{\sigma_0}$ by exciting the plate with higher pump amplitude.

To improve signal-to-noise ratio of the previous image, the number of receivers was increased up to $N_r = 19$ and sources up to $N_s = 18$ (see Figure. 6-(left)). A localization result of this experiment is given in Figure. 6-(right). The virtual emitter is located at (0.724, 0.126) m, there are $M = 3900$ windows of duration $\Delta T = 10$ ms.

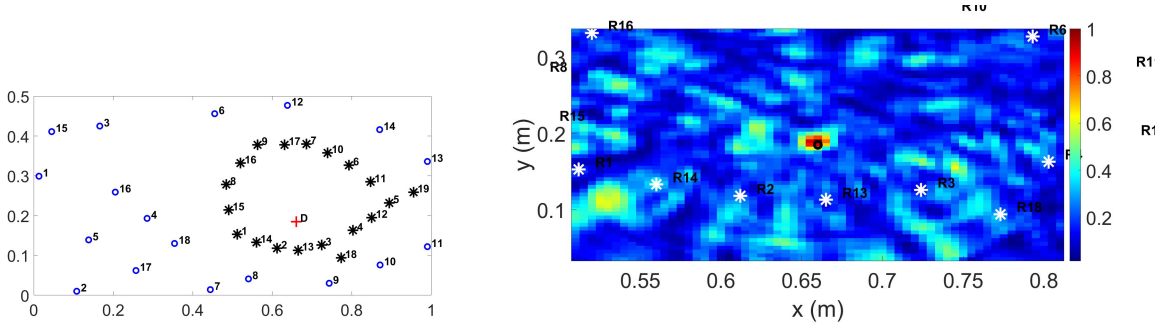

Figure 6. (Left) Schematic configuration of the considered experiment. (Right) Passive image of a CAN obtained with $N_s = 18$ and $N_r = 19$, located at (0.66,0.185) m. The circles denote noise emitters, the asterisks are for receivers and the cross represents defect position.

As we can observed, the defect is correctly localized.

4. Wrap-up

The work presented here establishes the concept of energy transferring from ambient low-frequency vibrations towards a secondary high-frequency noise field by exploiting the dry contact frictional nonlinearities. The device consists in a mechanical system composed by a primary

resonator, which is tuned to the low frequency (LF) structural vibrations of the plate, and a secondary resonator (flexible beam), which allows the transferring of HF vibrations. The acoustic HF noise generated by the devices has appeared to have non-negligible components in the useful frequency passive imaging range. In other part, we are interested to passive reference-free localization algorithm based on a combination of pump-probe experiment, Green's function retrieval from noise correlations and back-propagation is proposed as a proof of concept of passive dynamic SHM. Contact acoustic nonlinearity has been successfully detected. In future works, we will conduct a full and deep experimental study on using artificial secondary sources developed in section 2 with passive dynamic contact non linearity imaging. This could of great interest for SHM applications.

4.1. Acknowledgments

This work has been supported by the French National Research Agency (ANR) grants: PASNI and PANSCAN Project, and by LABEX WIFI (Laboratory of Excellence within the French Program "Investments for the Future") under reference ANR-10-IDEX-0001-02 PSL.

References

[1] O.I. Lobkis and R. Weaver. On the emergence of the Green's function in the correlations of a diffuse field. *J. Acous. Soc. Am*, 110:3011 – 3017, 2001.

[2] E. Larose, P. Roux, and M. Campillo. Reconstruction of Rayleigh-Lamb dispersion spectrum based on noise obtained from an air-jet forcing. *J. Acous. Soc. Am*, 122:3437 – 3444, 2007.

[3] K.G. Sabra, P. Roux, and W. A. Kuperman. Emergence rate of the time- domain Green's function from the ambient noise cross-correlation function. *J. Acous. Soc. Am*, 118:3524 – 3531, 2005.

[4] K.G. Sabra, E. S. Winkel, D. A. Bourgoyne, B. R. Elbing, S. L. Ceccio, M. Perlin, and D. R. Dowling. Using cross-correlations of turbulent flow-induced ambient vibrations to estimate the structural impulse response. Application to structural health monitoring. *J. Acous. Soc. Am*, 121:1987 – 2005, 2007.

[5] E. Moulin, N. Abou Leyla, J. Assaad, and S. Grondel. Applicability of acoustic noise correlation for structural health monitoring in nondiffuse field conditions. *Appl. Phys. Lett*, 95:094104 – 094104–3, 2009.

[6] M. Davy, J. De Rosny, and M. Fink. Green's function retrieval and passive imaging from correlations of wideband thermal radiations. *Phys. Rev. Lett*, 110:203901, 2013.

[7] T. Nowakowski, L. Daudet, and J. de Rosny. Localization of acoustic sensors from passive Green's function estimation. *J. Acous. Soc. Am*, 138:3010 – 3018, 2014.

[8] L. Chehami, E. Moulin, J. de Rosny, C. Prada, O. Bou Matar, F. Benmeddour, and J. Assaad. Detection and localization of a defect in a reverberant plate using acoustic field correlation. *J. App. Phys*, 115:104901–1: 104901–7, 2014.

[9] L. Chehami, J. de Rosny, C. Prada, E. Moulin, and J. Assaad. Experimental study of passive defect localization in plates using ambient noise. *IEEE Trans. Ultrason. Ferroelectr. Freq. Control*, 62:1544–1553, 2015.

[10] Guangzhi Chen, Damien Pageot, Odile Abraham, Yuxiang Zhang, Mathieu Chekroun, and Vincent Tournat. Nonlinear coda wave interferometry: Sensitivity to wave-induced material property changes analyzed via numerical simulations in 2d. *Ultrasonics*, 99:105968, November 2019.

[11] K. C. Gryllias, E. Chatelet, Fr. Massi, and E. Moulin. Energy transfer between aacoustic fields by dry frictional contacts for SHM: a lumped numerical analysis. *Proceedings - ISMA (KU Leuven, Belgium)*, 2014.

[12] Lynda Chehami, Emmanuel Moulin, Julien de Rosny, Claire Prada, Eric Chatelet, Giovanna Lacerra, Konstantinos Gryllias, and Francesco Massi. Nonlinear secondary noise sources for passive defect detection using ultrasound sensors. *Journal of Sound and Vibration*, 386:283–294, January 2017.

[13] A. Akay. Acoustics of friction. *J. Acous. Soc. Am*, 111:1525 – 1548, 2002.

[14] M. Terzi, L. Chehami, M. Farin, E. Moulin, V. Aleshin, N. Smagin, J. de Rosny, and F. Benmeddour. Pump-probe localization technique of varying solid contacts. *The Journal of the Acoustical Society of America*, 149(5):2943–2949, May 2021.

[15] Lynda Chehami, Emmanuel Moulin, Julien de Rosny, and Claire Prada. Accuracy of greens function estimation from correlation of diffuse elastic waves on thin plates. *The Journal of the Acoustical Society of America*, 146(5):3505–3511, November 2019.

[16] Marina Terzi. *Ultrasonic imaging of contact defects under low frequency loading: application for structural health monitoring of elastic plates.* PhD thesis, Université Polytechnique Hauts de France, 2022.